Modelling the high-resolution dynamic exposure to flood in city-region

Xuehong Zhu[1], Qiang Dai[1, 2, 4, *], Dawei Han[2], Lu Zhuo[2], Shaonan Zhu[3], Shuliang Zhang[1, *]

[1]Key Laboratory of VGE of Ministry of Education, Nanjing Normal University, Nanjing, China

[2]WEMRC, Department of Civil Engineering, University of Bristol, Bristol, UK

[3]College of Geographical and Biological Information, Nanjing University of Posts and Telecommunications, Nanjing, China

[4]Jiangsu Center for Collaborative Innovation in Geographical Information Resource Development and Application, Nanjing, China

*Correspondence: qd_gis@163.com

Abstract:

Urban flooding exposure is generally investigated with the assumption of stationary disasters and disaster-hit bodies during an event, and thus cannot satisfy the increasingly elaborate modelling and management of urban floods. In this study, a comprehensive method was proposed to simulate dynamic exposure to urban flooding considering residents' travel behavior. First, a flood simulation was conducted using the LISFLOOD-FP model to predict the spatio-temporal distribution of flooding. Second, an agent-based model was used to simulate residents' movements during the urban flooding period. Finally, to study the evolution and patterns of urban flooding exposure, the exposure of population, roads, and buildings to urban flooding was simulated using Lishui, China as a case study. The results showed that water depth was the major factor affecting total urban exposure in Lishui. Urban exposure to fluvial flooding was concentrated along the river, while exposure to pluvial flooding was dispersed throughout the area (independent from the river). Additionally, the population distribution on weekends was more variable than on weekdays and was more sensitive to floods. In addition, residents' response behavior (based on their subjective consciousness) may result in increased overall exposure. This study presents the first fully formulated method for dynamic urban flood exposure simulation at a high spatio-temporal

resolution. The quantitative results of this study can provide fundamental information for urban flood disaster vulnerability assessment, socioeconomic loss assessment, urban disaster risk management, and emergency response plan establishment.

Keywords: urban flooding; resident travel behavior; agent-based model; dynamic exposure

1. Introduction

Storm flooding has become increasingly frequent and severe with the intensification of global warming and the rising frequency of extreme weather events (*Dankers and Feyen, 2008*; *Hammond et al., 2015*). Urban floods have become major natural disasters in many cities around the world and have created serious threats to human life and social and economic activities (*Gain et al., 2015*). Effectively coping with floods and their adverse effects is an important part of disaster prevention and mitigation as well as disaster risk management (*Atta-Ur-Rahman, 2014*). Non-engineering measures such as exposure assessment are currently the main way of managing urban flooding risk (*Chen et al., 2015*). Exposure refers to the presence of people, livelihoods, environmental services and resources, infrastructure, or economic, social, or cultural assets in places that could be adversely affected by natural disasters (*IPCC, 2012*). Urban flood disasters are caused by the adverse effects of heavy rain and other factors on the city system in certain disaster-prone environments. These events consist of three parts: disaster-causing factors, disaster-prone environments, and disaster-hit bodies (*Shi, 1996*).

The characteristics of flood disasters and building environments and the distribution of population and socio-economic resources are the key factors for evaluating urban flood exposure due to the dynamic evolution of urban floods and disaster-hit bodies. The methods used for evaluating exposure to urban flooding at a certain time or period vary due to changes in the disaster-hit bodies,

study areas, and data acquisition methods (*Röthlisberger et al., 2017*). Index-based methods are commonly used for comprehensive exposure evaluation (*Mahe et al., 2005*; *Mansur et al., 2016*; *Guo et al., 2014*). Statistical methods based on historical disaster data are also utilized (*Moel et al., 2011*).

With respect to spatial considerations, the currently implemented method for estimation of disaster exposure adopts the administrative boundaries of socioeconomic data, which are organized as research units (*Yin, 2009*). Consequently, natural elements that have higher spatial resolutions must be compromised due to the lower spatial resolution of human elements like population (*Yang et al., 2013*). Therefore, a comprehensive and sophisticated geographic research unit has not been established, thus resulting in simulation results applicable only to macro-scale planning and decision making. Hence, the estimation of disaster exposure needs to incorporate greater spatial heterogeneity and resolution.

Besides enhancement of the spatial scale, dynamic temporal simulation of disaster exposure has gained increasing attention. Specifically, the dynamic evolution of disaster exposure at the macro time scale considers exposure distribution as well as its variation during different development periods (*Weis et al., 2016*). Therefore, this method is relatively mature and has led to abundant research results. At the micro time scale, disaster-causing factors and disaster-hit bodies represented by populations are constantly varying. On one hand, spatio-temporal changes in disaster-causing factors (rainfall) result in corresponding dynamic changes in the characteristics (water depth and velocity) of urban flood disasters. On the other hand, daily travel activities of urban residents, such as commuting between residential and work or study areas, cause a dynamic spatio-temporal distribution of the population. At the same time, the exposure to urban flooding changes dramatically over a short period of time. To avoid or reduce disaster risks, casualties, and

property losses, different individuals are likely to adopt different adaptive behaviors, such as delaying or cancelling travel plans, while the government is likely to adopt organizational actions such as issuing warnings and evacuating residents (*Wan and Wang, 2017*; *Parker et al., 1995*). Thus, the dynamic simulation of exposure requires the dynamic space-time simulation of variations in the disaster, and disaster-hit bodies, as well as interactions between them.

Modelling of the spatio-temporal changes in natural disasters mainly uses the disaster system simulation method (*Werren et al., 2016*). A wide variety of existing hydrological or hydrodynamic models capable of simulating fluvial or pluvial flooding are available, including the Storm Water Management Model (SWMM) (*Rossman, 2015*), LISFLOOD (*Bates and De Roo, 2000*), MIKE-SHE (*DHI, 2000*), MIKE-11 (*Havnø et al., 1995*), MOUSE (*Lindberg et al., 1989*), HEC-RAS (*Brunner, 2008*), and HEC-HMS (*Charley et al., 1995*). Change simulations of the disaster-hit body (population) can use methods based on individual spatio-temporal data (*Liang et al., 2015*). Although this can acquire human positions and movement tracks, it is difficult to identify the purpose of human activities, such that human disaster response behavior cannot be accurately simulated.

Some modelling techniques, often collectively referred to as social simulation, have been successfully used to represent the behaviors of humans and organizations. These include event and fault trees, Bayesian networks, microsimulation, cellular automata, system dynamics, and agent-based models (ABMs). Research methods based on ABMs have been gradually introduced to the field of natural disaster risk assessment as these can simulate population distribution as well as interactions among the population (as the disaster victims), hazard factors, and disaster-prone environments (*Yin, et al., 2016b*). Current research has used the ABM to simulate human responses to disasters, which, in turn, have been used in natural disaster risk research (*Johnstone, 2012*;

Huang et al., 2015). Nevertheless, the simulation results do not reflect the exposure characteristics of the disaster-hit bodies and their dynamic changes (*Dawson et al., 2011*).

Therefore, the objectives of this study were to develop a novel method using the LISFLOOD-FP model (Sect. 3.1) and an ABM (Sect. 3.2) to simulate the exposure of urban populations, roads, and buildings to flooding under varying conditions and subsequently implement the method as a pilot in a real city. Several scenarios, including diverse flooding types and various responses of residents to flooding, were considered in this regard. Additionally, dynamic features of the real world were incorporated to improve the micro exposure analysis. This method was subsequently applied to an urban area as a case study. Exposure simulation is a useful tool for estimating disaster vulnerability and assessing losses, and the quantitative results under different scenarios of this study are likely to benefit relevant government agencies in assessing risk, issuing warnings, and planning emergency responses to urban natural disasters. In particular, considering the dynamic distribution of the population under flooding, a more reasonable mitigation measure can be taken to minimize casualties.

2. Study area and data source

In this study, Lishui City in Zhejiang Province, China, was considered as the study region because of the availability of the required data and flooding history. The urban district of Lishui is a largely hilly and mountainous area, and the Oujiang River traverses its southern and eastern parts. The study area is located in the central district of Lishui, covers an area of 43.4 km^2, and has a large population of about 71673 (Fig. 1). The frequencies of heavy rainstorms and persistent concentrated rainfall events rise sharply in May and June during the Meiyu flood period, which

115 often results in flood disasters. On August 20, 2014, a heavy rainfall event lasting a few days
116 produced a 50-year flood in Lishui and caused considerable loss of property.

117 The datasets used in this study included a digital elevation model, rivers, roads, buildings,
118 population, and observation data consisting of river discharge and water level. Travel survey data
119 from a questionnaire (see Supplementary Material) were used to generate daily routines.
120 Additionally, traffic flow and water accumulation data were used for validation. Table 1 describes
121 the sources and uses of the datasets.

122 The travel survey data used in this study were taken from a face-to-face questionnaire survey
123 conducted from July 8, 2018 to July 14, 2018. A total of 25 subdistricts were selected based on
124 sample selection. According to the distribution of the subdistricts, the investigators were divided
125 into five groups of at least four investigators per group. In each group, a senior researcher
126 monitored the survey process, coordinated questionnaire collection and checked the completeness
127 and validity of the questionnaires collected. Before each interview, the investigators explained the
128 purpose of the investigation and confidentiality principles. The respondents in the study
129 participated voluntarily, and were allotted enough time to answer the questionnaire. In total, 623
130 questionnaires were distributed, 589 were collected, and 500 valid responses were selected after
131 excluding incomplete questionnaires (the response rate was 80.3%). The distribution of the social
132 characteristics of the respondents coincided with the actual population distribution in the study
133 area.

134 **3. Methodology**

135 This study comprised three aspects: disaster simulation, human activity simulation, and dynamic
136 exposure assessment (Fig. 2). The first step included fluvial and pluvial flooding simulation based

on the LISFLOOD-FP model. The simulation of human activity utilized ABM to obtain the spatio-temporal distribution of the population under different scenarios. Finally, the developed model was combined with the results of the previous two steps to assess the dynamic exposure of the population, roads, and buildings to urban flooding.

3.1 Flood models

LISFLOOD-FP (*Bates et al., 2013*) is a coupled 1D/2D hydraulic model based on a raster grid and was designed for research purposes at the University of Bristol. LISFLOOD-FP uses a square grid as the computational grid to simulate one-dimensional river hydraulic changes and two-dimensional floodplain hydraulic changes. The applicability of the model has been verified by several studies (*Horritt and Bates, 2002*; *Bates and De Roo, 2000*). Therefore, the LISFLOOD-FP model was chosen for the simulation of fluvial and pluvial flooding.

Floodplain flows were described in terms of the continuity and momentum equations discretized over a grid of square cells, which allowed the model to represent 2D dynamic flow fields for the floodplain. It assumed that the flow between two cells was simply a function of the free surface height difference between those cells:

$$\frac{dh^{i,j}}{dt} = \frac{Q_x^{i-1,j} - Q_x^{i,j} + Q_y^{i,j-1} - Q_y^{i,j}}{\Delta x \Delta y}, \quad (1)$$

$$Q_x^{i,j} = \frac{h_{flow}^{5/3}}{n}\left(\frac{h^{i-1,j} - h^{i,j}}{\Delta x}\right)^{1/2} \Delta y, \quad (2)$$

where $h^{i,j}$ is the free surface height of water at node (i,j), Δx and Δy are the cell dimensions, n is the effective grid scale Manning's friction coefficient for the floodplain, and Q_x and Q_y describe the volumetric flow rates between the floodplain cells in the x and y directions, respectively. The

157 flow depth, h_{flow}, represents the depth through which water can flow between two cells, and d is
158 defined as the difference between the highest free surface height of water in the two cells and the
159 highest bed elevation.

160 The types of flooding simulated in this study included pluvial and fluvial floods. The input of the
161 model included DEM, rainfall, channel, and floodplain friction data. When it comes to fluvial
162 flooding simulations, boundary conditions, including river, water level, and river discharge were
163 also needed. The output data were water depth and water velocity in the x and y directions,
164 respectively. Due to the lack of hourly rainfall observation data, we used designed rainfall data for
165 pluvial flood simulation (*Dai et al., 2015*). Synthetic rainfall data for a return period of 50 years
166 were simulated using the Chicago hyetograph method (CHM) (*Cen et al., 1998; Dai et al., 2014*).
167 The rainfall data were determined using the rainstorm intensity formula (Eq. (3)), rainfall duration
168 time, and peak position (*r*).

169 $$i = \frac{A(1+c\log P)}{167(t+b)^n}, \quad (3)$$

170 where i is the rainfall intensity (mm/min), P is the return period, and t is the time. A, b, c and n
171 are parameters related to the characteristics of the local rainstorm and need solutions. A is the
172 rainfall parameter, i.e. the design rainfall (mm) for 1 min at a 10 year return period, c is the rainfall
173 variation parameter (dimensionless), and b is the rainfall duration correction parameter, i.e. the
174 time constant (min) that can be added to convert the curve into a straight line after logarithmic
175 calculation of the two sides of the rainstorm intensity formula. n is the rainstorm attenuation index,
176 which is related to the return period. The *r* refers to the relative rainfall peak time, i.e., the value
177 from zero to one. Zero means the maximum rainfall at the beginning of rainfall and one means the
178 maximum rainfall at the end of rainfall. To simulate the flood in 2014, we fixed *r* at 0.2 based on

the assumption that the peak is located at the one fifth point of the design hyetograph. Additionally, the rainfall duration was 6 hours (6 am to 12 pm), and the accumulated rainfall was 148.59 mm. The parameters A, b, c and n were estimated from the rainstorm intensity formula for Lishui City obtained from the "Zhejiang City Rainstorm Intensity Formula Table" published by the Hangzhou Municipal Planning Bureau (Table 2). The rainfall simulation results are shown in Fig. 3(a). The river discharge and water level input data for fluvial flood simulation utilized observational data from Lishui's 50-year flood in 2014, provided by the Liandu Hydrological Station (Fig. 3(b)). The flow data for the Daxi and Haoxi Rivers on August 20, 2014 were obtained from the Xiaobaiyan and Huangdu stations, respectively, and the observational data for water levels at the outlets were those for the Kaitan Dam.

3.2 Spatio-temporal simulation of population distribution

An ABM is a computational method for simulating the actions and interactions of autonomous decision-making entities in a network or system to subsequently assess their effects on the system as a whole. Individuals and organizations represent agents, each of which individually assesses its situation and makes decisions based on a set of rules. Agents may execute various behaviors appropriate for the system component they represent (such as producing or consuming). Therefore, an ABM consists of a system of agents and the relationships between them. Even a simple ABM can exhibit complex behavior patterns because a series of simple interactions between individuals may result in more complex system-scale outcomes that could not have been predicted just by aggregating individual agent behaviors. The ABM of residents' travels established in this study included two core elements (agents and activities) and two basic elements (blocks and networks). Individual movements were simulated by defining the activity patterns of different types of residents, allowing us to obtain the distribution of the population at each moment.

Residents were independent individuals with subjectivity, abstracted as agents in this study. Only a limited number of agent classifications were used to reduce the number of agent types. The types of agents were classified according to the social characteristics of the residents. Age and gender characteristics mainly affect the ability of people to respond to disasters. The self-help abilities of minors under 18 years of age and residents older than 60 years are generally poor. In the event of natural disasters, they are generally categorized as the objects of help. The middle-aged group (18–60 years old) generally has greater physical strength with a better ability to cope with disasters. Unemployed people are more vulnerable to natural disasters. On one hand, their living environments and resistance to disasters are poor; on the other hand, their economic conditions are limited, which impedes recovery after the disaster and seriously affects their daily life in the short term. Education level is related to the possibility of receiving early warning information by the individual. Individuals with higher education levels are more likely to respond to early warning information and are more aware of disasters than others (*Terti et al., 2015*; *Shabou et al., 2017*). Additionally, different travel modes have different effects on the activity patterns of people as well as on exposure levels when disasters occur. Therefore, the agent types were divided according to age, gender, employment status, education level, and travel mode.

Activities were classified as work, study, recreation, shopping, at-home, and travel. An activity pattern consisted of a series of activities to describe the spatio-temporal distribution of the agent. The location and scope of an agent were restricted to blocks and networks. Different types of agents indicated different activity patterns, and the same agent type could also indicate different activity patterns in different scenarios. The travel survey data were used according to the demographic properties of the agent to generate synthetic daily routines. To capture the variability in the travel survey and the uncertainties in behavior, synthetic daily routines were described in

probabilistic terms based on the activity patterns derived from survey data. The probability of residents' activity patterns was estimated by (1) classifying residents according to their social characteristics, (2) summarizing their daily activity patterns and estimating the probability of each activity, and (3) using their reported flood risk perception to calculate expected changes in activity patterns during disaster scenarios and estimate the probability of different responses being taken by different types of residents. Figure 4 presents an example of the synthetic daily routine of an agent with the following demographic characteristics: male agent, aged 18–60 years, and employed. In this example, the agent started the day at 8 am on a weekday. The agent then had a 0.8 probability of going straight to work, subsequently went home, and so on.

The study area was discretized into many blocks to improve the spatial resolution of the exposure results. The major factors that affect the flood exposure are considered, including rivers, roads, land use, and buildings. The discretization procedure was conducted with geographic information system (GIS) tools (intersection and editing tools of the ArcGIS software) (*Lü et al., 2018*). Blocks, the smallest unit of exposure, were defined as activity locations for agents and were divided into five categories: residential area, school, company, recreational area, and river. Residential areas were subdivided into classes I, II, III, and IV according to the type of building.

In this study, the network referred to roads and restricted the spatial travel scope of an intelligent agent. Rural roads, highways, and urban roads (including main roads, sub trunk roads, and its branches) were included in the network. The route selection criteria were defined once the different activities from each individual's schedule were located, and road section attributes were specified. Although various factors are involved in the route selection process, several studies have indicated that minimizing travel time is the principal criterion (*Papinski et al., 2009*; *Ramming, 2001*; *Bekhor et al., 2006*). Here, a simple but effective shortest path method was used. The classical Dijkstra

algorithm is a single-source shortest path algorithm that provides trees of minimal total length and time in a connected set of nodes (*Dijkstra, 1959*). The activity pattern attributions concerned only the starting times and durations of the activity sequences, thus indicating that the travel duration for each individual was computed based on the distance between the different activity locations. Therefore, the implemented schedules may be distorted compared to the assigned schedules in terms of travel durations (*Terti et al., 2015*). We can get the departure and destination block of each stage according to the activity patterns, and then calculate the shortest path consisting of a series of road sections. At each moment, the block in which the agent is located is calculated. If on the road, according to differences in the speed of walking, riding a bus, or driving a car, the road section location is calculated. During flooding, this is similar in every aspect except the activity patterns.

3.3 Impacts of disasters on anthropogenic activities

This study accounted for the adaptability or adjustment behavior of residents to disasters during the disaster event. The type of activity and its sensitivity to disaster affected the residents' disaster response behavior. Recreation and shopping activities were easier to cancel and postpone than work and study (*Cools et al., 2010*). The sensitivities of residents to disasters depended on their socioeconomic characteristics and risk factors such as disaster- (flood-) related knowledge and experience. People with higher education levels are more knowledgeable about disasters and are more likely to receive early warning information and take effective measures (*Terti et al., 2015*). Additionally, it is easier for workers to ignore the risks of a disaster (*Ruin et al., 2007*; *Drobot et al., 2007*). Therefore, this study accounted for the impacts of education level on the response behavior of residents to disaster events.

The impacts of a disaster on population distribution were determined by defining different activity patterns and their changing probabilities. Figure 5 shows activity patterns during different disaster scenarios for employed adult men who had received higher education. The “bad weather” scenario was similar to the “daily activity” pattern. For instance, the change in travel probability during “bad weather” due to a rainstorm reflected the adaptive behavior of residents. The “warning” scenario assumed that the government had issued early warning information at 8 a.m., that schools had suspended classes on weekdays, and the resident responses were stronger than those to the “bad weather” scenario, thereby resulting in a greater difference in activity patterns.

3.4 Dynamic exposure assessment

The dynamic exposure was calculated based on the simulations of spatio-temporal distributions of the population and flooding. Therefore, the exposure at each moment was calculated according to the population distribution and flood data at that time. Based on the data availability, this study focused only on three types of disaster-hit bodies, i.e., population, roads, and buildings.

(i) Population

Population exposure generally refers to the population exposed to the impacts of disaster events and is characterized by regional population size or density. This study selected the exposed population and accounted for vulnerable groups and road users. Age was the primary factor impacting vulnerability. Specifically, the young (people under the age of 18 years) and the elderly (people over 60 years old) were the vulnerable groups.

(ii) Roads

As the basic skeleton of a city, roads are not only the media for daily travel of passengers and freight transportation but also disaster-hit bodies (*Yin, et al., 2016a*), as they are vulnerable to flood disasters. This study selected the number and lengths of exposed roads to reflect road exposure.

(iii) Buildings

Aggravation of urban flooding has made building flooding more common in urban areas, resulting in loss of internal property and construction structure. Additionally, the dynamic state of building exposure is related to the safety of both the building as well as the surrounding population. In this study, the area of the exposed building and the depth of accumulated water in the building were considered as the building exposure.

3.5 Scenario design

The daily behaviors of people are characterized by certain patterns with regard to daily, weekly, monthly, and annual cycles. The rainstorm ("bad weather") and disaster response measures adopted by the organization ("warning") are likely to affect people's daily behaviors. Therefore, 12 scenarios, representing different flooding types and human activities, were designed in this study (Table 3). S1, S2, S7, and S8 were control groups that indicated human activity with no rain and no warning, while the rest of the scenarios were experimental groups.

3.6 Model implementation and parameter setting

GIS, an important spatial data management and analysis technology, plays an important role in dynamic exposure analysis of urban floods. In addition, the Python programming language is being increasingly adopted by researchers due to its simplicity, readability, and flexible usability. Therefore, the model was developed using the Visual Studio Code software (*Visual studio code,*

311 *2018*) and Python programming language (*Python*, *2018*). The development of the graphical user
312 interface (GUI), GIS module, and drawing module used Qt (*Qt, 2018*), Geopandas (*Geopandas,*
313 *2018*), and Matplotlib (*Matplotlib, 2018*), respectively.

314 (i) Block generation

315 Blocks are irregular vector units whose size represents spatial resolution. Therefore, the spatial
316 resolution of the results is related to the study area and data. In this study, the study area was
317 divided into 237 blocks based on the method introduced in Sect. 3.3, with a minimum area of
318 2731.64 square meters. The block types and their spatial distributions are shown in Fig. 6 and Fig.
319 7, respectively. Most of the blocks in the study area were categorized as residential area, while
320 blocks of recreational areas were few and concentrated.

321 (ii) Parameter setting

322 To reduce the number of agent types, only a limited number of agent classes were used. The
323 distribution of population characteristics for Liandu District is shown in Table 4. The agents were
324 divided into 18 types for normal daily (non-disaster) scenarios (S1, S2, S7, and S8) and 24 types
325 for disaster scenarios (other scenarios except S1, S2, S7, and S8) based on the influence of
326 education level on the individual disaster response behavior (Fig. 8).

327 Since the census data did not identify individuals by address, each simulation began by creating
328 an agent population with the same distributions of age, gender, employment, education level, and
329 travel mode that was randomly located within the residential area. The synthetic daily routines
330 were described in probabilistic terms to capture the variability present in the travel survey and
331 other uncertainties in behavior. The probabilities of all daily activities for all agents were generated
332 based on the travel survey.

(iii) Exposure threshold

Although flood fatalities can occur through a number of mechanisms, such as physical trauma, heart attack, or electrocution, drowning accounts for two-thirds of the fatalities (*Jonkman and Kelman, 2005*). Previous research has established that the probability of death or serious injury as a result of exposure to flooding (*Abt et al., 1989*; *Karvonen et al., 2000*; *Lind et al., 2004*; *Jonkman and Penning‐Rowsell, 2008*) is dominated by (1) the depth of floodwater and (2) the velocity of floodwater. Additionally, the rate of water level rise can also play an important role in this regard. However, other factors, such as age, fitness level, height, and weight of the individual, are also important for determining their vulnerability to disasters. A comprehensive review of flood-related casualty data and methods used to assess the risk of death or serious harm caused by flooding was provided by the *Department for Environment Food and Rural Affairs and Environment Agency (2003)* and *Jonkman and Penning‐Rowsell (2008)*. In this study, rather than predicting mortality (which is subject to random factors as well as those mentioned previously), exposure to floodwater depths of 25 cm or greater under relatively fast flowing (2.5 m/s or greater) conditions was established as the threshold for the most vulnerable people (*DEFRA and Environment Agency, 2003*). This provided a conservative estimate of individuals vulnerable to floodwater rather than an estimate of mortality (*Dawson et al., 2011*).

Since building steps (thresholds) exert a blocking effect on shallow flooding, they are likely to reduce the degree of flooding by restricting the flood water to the outside of the building, thereby reducing the exposure of the building. Therefore, this study assigned building step height to corresponding block types according to the architectural design standards of China and the actual conditions of the study area (Table 5). Therefore, the exposure of the building was determined

according to the depth of the flood and the height of the building steps. The depth of the water entering the building was the difference between the depth of the flood and the height of the steps.

4. Results

4.1 Flood simulation

The temporal resolution of flood simulation results was unified with other output results for half an hour. Figure 9 indicates the accumulated water depths and velocities of pluvial and fluvial floods in the study area. As is evident, the pluvial and fluvial floods exerted significant impacts, and the urban area near the Oujiang River was the most severely flooded. Additionally, water also accumulated in the inner areas of the city, mainly on roads, in case of pluvial flood disasters. The variations in water depth and velocity for seven severely flooded areas (including blocks and roads) are presented in Fig. 10. Evident spatio-temporal variations in flooding were observed and water depth was the major factor affecting the total urban exposure to flooding in Lishui.

The flood simulation results were indirectly validated by actual water accumulation points. During the 50-year flood in 2014, the city had 10 flooded roads and 18 water accumulation points. The actual hydrological points selected according to the study area and the urban flooding results simulated by the prototype system are indicated in Fig. 11.

To avoid overlapping with the simulated water accumulation results for roads, the actual flooding points in the figure only included road junctions, and the entirety of Gucheng Road (Lutang Street to Dayou Street section) and Liyang Street (which connected the senior middle school to the Sanyan Temple section) was represented by corresponding intersection points. Figure 11 indicates that both the simulation results and the actual water accumulation points were mainly distributed along the river. The simulated water accumulation area (Fig. 11(a)) included roads in the center of

the city and was larger than the actual flooding area. This difference could be attributed to different definitions of "water accumulation". The simulation results presented in Figure 11 included all areas where the accumulated water depth during the flooding period was greater than 15 cm. The actual water accumulation point was defined as one experiencing rainfall greater than 50 mm over a 24 hour period. Additionally, it was characterized by the water accumulation depth of the road reaching 15 cm (the meteorological department issued a blue rainstorm warning at this level), the water withdrawal time reaching one hour, and the water accumulation scope value being greater than 50 m^2. Certain gaps existed between the observational data and the actual river discharge since the observation station was far from the study area. Hence, the results indicated that the simulated water accumulation area during the fluvial flood (Fig. 11 (b)) was smaller than that of the actual situation.

4.2 Simulation of the spatio-temporal distribution of population

The spatial and temporal resolutions of the modelling results could be adapted to the study area. The area of the minimum block was 2731.64 m^2. The temporal resolution of the results was half an hour, which could be set to 10 minutes or even 1 minute according to the requirements. Additionally, no accurate traffic model was used to simulate agents' movements on road for two reasons: (1) to improve efficiency and (2) we did not pay attention to high temporal-resolution human movements (such as one minute or one second), but only focused on the population distribution for a period of time, so the temporal resolution requirement of human activities was low.

The spatio-temporal population distribution was simulated based on six scenarios: (1) daily, weekday (S1, S7); (2) daily, weekend (S2, S8); (3) bad weather, weekday (S3, S9); (4) bad weather,

399 weekend (S4, S10); (5) warning, weekday (S5, S11); (6) warning, weekend (S6, S12). Figure 12
400 indicates the population variation for blocks and roads for the six scenarios. Figure 12(a) indicates
401 that, among the three weekend scenarios, the population in the playground (Block 77) changed
402 more than the population in the company (Block 113). Figure 12(b) indicates that the population
403 on the roads was volatile, and the morning peak hour during the weekend was delayed by an hour
404 in comparison to that during the weekdays. The population distribution in the study area is shown
405 in Fig. 13. The population was unevenly distributed and concentrated in recreational and
406 residential areas over the weekend. However, the population distribution on weekdays was
407 relatively uniform. The population distribution on weekends was more variable than that on
408 weekdays and was more sensitive to floods. The concurrent population distribution for the six
409 scenarios changed significantly during the weekend, while the distribution for weekdays changed
410 little.

411 Figures 12 and 13 indicate that the population change patterns were different for different blocks
412 types. The daily routines of most people started from the residential area (home) in the morning,
413 followed by school or company blocks during weekdays and recreational areas during weekends,
414 and, finally, concluded with a return to the residential area at night. During the occurrence of
415 rainstorms or the reception of warning messages, different types of people reacted differently
416 (continuing, postponing, or cancelling the originally planned activities). Vulnerable people, such
417 as the elderly and children, and sensitive people, such as the homeless, were more likely to cancel
418 travel plans. Additionally, recreational activities were more likely to be cancelled than were study
419 and work activities.

420 The reliability of the simulation of the spatio-temporal population distribution was indirectly
421 verified by utilizing traffic flow data. Due to the lack of data for 2014, we used traffic flow data

from June 24 to July 7, 2017. The simulated total number of residents passing the four intersections (such as the junction of the Liqing and Huayuan roads) and the actual measured traffic flow at the intersections during the morning and evening peak hours on weekdays and weekends are shown in Table 6 and Table 7, where "Sim." means simulation results, "Obs." means measured values (multi-day average results), "LQ" is Liqing Road, "KF" is Kaifa Road, "HY" is Huayuan Road, "ZJ" is Zijin Road, and "LT" is Lutang Street. The deviation ratio was calculated as: (Sim. – Obs.) / Obs.

In theory, the simulated value should be much larger than the measured value since the former indicates the number of people while the latter represents the number of cars and buses. However, as indicated in Table 6 and Table 7, the simulated value was close to the measured value. This could be attributed to the assumption that the study area was closed and the simulated population was the number of permanent residents, excluding the migrant population. In reality, the number of migrants in the urban area during daytime is large owing to its geographical location. Moreover, this study simplified human activities when simulating the spatio-temporal distribution of the population. Therefore, the number of pedestrians on the road was small. However, there was a deviation ratio of about ±5% between the simulated value and the measured value, except for three deviation ratios of about ±10%. Therefore, the simulation method for the spatio-temporal distribution of population is feasible, and the results are reliable.

4.3 Dynamic exposure assessment

Figure 14 presents the population exposure variation for two selected areas. The difference between pluvial and fluvial flood scenarios could be attributed to differences in the changes and degrees of water accumulation. Figure 14(a) indicates that population exposure was the highest for

444 the daily scenario, followed by the bad weather scenario and minimum warning scenario. However,
445 as indicated in Fig. 14(b), the population was most exposed to both weekend and weekday warning
446 scenarios. This is due to the assumption that the disaster response behavior adopted by residents
447 was to reduce travel, i.e., the refuge of residents was the residential area. Additionally, the response
448 was not based on the exposure of the residential area. Therefore, when residential areas, such as
449 Block 6, were exposed to floods, the residents chose to reduce travel, thus resulting in an increase
450 in the population of residential areas and consequently increasing the population exposure. Thus,
451 if the government informs the residents of Block 6 in advance about the location of appropriate
452 shelters, the exposed population will be effectively reduced. The method proposed in this study
453 can also help determine vulnerable populations and road users in the exposed blocks.

454 Figure 15 presents variations in the road and building exposures of two selected areas with serious
455 flooding. The road and building exposures for the study area are presented in Fig. 16. It can be
456 concluded that road and building exposures during pluvial and fluvial floods also varied with the
457 flood depth. The urban area exposed to fluvial floods was concentrated along the river, while that
458 exposed to pluvial floods was relatively dispersed and independent. Additionally, the exposed road
459 length of the block fluctuated, while the buildings were either entirely exposed or not exposed.
460 Furthermore, the area of the road affected by pluvial and fluvial floods was greater than that of the
461 buildings. As indicated in Fig. 16, exposed buildings were present only in a few areas (3 blocks
462 for pluvial flood and 4 blocks for fluvial flood), while roads were affected in several areas (19
463 blocks for pluvial flood and 15 blocks for fluvial flood). In addition, buildings were the least
464 exposed due to high thresholds or the number of building steps designed and built in recent years,
465 while roads and population were severely affected by floods.

466 **5. Discussion and conclusions**

Urban flooding considerably impacts the life of residents, in terms of both daily commuting and casualties. This study proposed a method for obtaining high-resolution dynamic exposure to urban flooding. First, the spatio-temporal distributions of pluvial and fluvial floods were simulated by the LISFLOOD-FP model. Second, the responses of residents to bad weather and government measures (warnings) were incorporated to develop an ABM to simulate residents' activities during flooding. Finally, urban exposure during different flood scenarios was comprehensively simulated and was based on the population and hydrological simulation results, road and building data, and the case study of the Lishui urban district.

The high-resolution dynamic exposure of population, roads, and buildings to flooding estimated using the proposed method can play a significant role in assessing hazard risk and loss, thus supporting government efforts toward disaster risk management. As flood exposure constantly changes over short periods of time, such simulations allow the government to reasonably formulate emergency plans to minimize casualties and property losses while providing effective reference information for residents.

This study had four major findings. First, water depth was the major factor affecting total urban exposure to flooding in Lishui. Second, the population distribution on weekends was more variable than that on weekdays and was more sensitive to floods. Third, urban areas exposed to fluvial floods were concentrated along the river, while those to pluvial floods were relatively dispersed and independent. Roads had more blocks exposed to fluvial floods (8%) than pluvial floods (6%). Fourth, staying home was not the best individual choice, so residents' response behavior based on their subjective consciousness may result in increased overall exposure. This suggests that simple governmental alerts relating to the occurrence of urban flooding are insufficient for reducing urban exposure to flood hazards.

It should be noted that there is no comprehensive way to verify the proposed method because parameters of human behavior and psychological processes are difficult (or, to some extent, impossible) to obtain. In this study, the proposed method was verified indirectly. The actual traffic information for each road intersection was collected and compared with the simulated population results. Additionally, the information for actual water accumulation points was compared with the simulated water accumulation results.

However, a few limitations persist. For instance, considerable uncertainties regarding the use and design of the ABM exist. These include differences in the responses of residents of the same type to disasters in the same scenario. Therefore, based on the survey data, we designed simplified activity patterns, which are consistent with the actual situation of the study area. Moreover, simplification of the behavior patterns and disaster responses of residents is inevitable, resulting in differences between the simulation results and reality.

Based on the analysis of the indirect validation results, we also found several problems. Since the migrant population and the exchange between the city and the outside were not considered, the simulated road population was small, so we needed to use real-time traffic data (such as taxi trajectories and card data from public transportation) to calibrate activity patterns to obtain more realistic population distribution results. Moreover, the actual water accumulation point information cannot be completely consistent with the simulation result because of its definition, therefore the simulation result can only be roughly verified. We need more abundant and accurate historical hazard data to fine-tune the flood simulation results. Our study focused more on the explorative method, while the result is just an application case. Due to the limitation of the study area and data, the current results are quite general in an early stage. The method proposed also has many areas in need of improvements, such as the design of ABM. Therefore, future studies should focus on

optimizing the proposed method and practical case studies, which may produce more informative results.

Data availability

The geography, hydrological observation, and traffic flow data in Lishui city were provided by Lishui City Housing and Urban-Rural Construction Bureau, Liandu Hydrological Station, and Lishui City Transportation Bureau, respectively. These data are not publicly available because of governmental restrictions. The 1 km grid population data are available online at http://www.geodata.cn (last access: March 2019). The population profile are available online at http://tjj.lishui.gov.cn (last access: March 2019). The water accumulation points are available online at http://www.zjjs.com.cn (last access: March 2019). Data provided by the local government and other model simulated data in this paper are available from the authors upon request (zhuxuehong816@163.com).

Author contributions

Xuehong Zhu and Qiang Dai were responsible for setting up the experiments, completing most of the experiments, and writing the manuscript. Dawei Han and Shuliang Zhang principally conceived the idea and design of the study and provided financial support. Lu Zhuo performed the flood simulation. Shaonan Zhu was responsible for the development of the model.

Competing interests

The authors declare that they have no conflict of interest.

Acknowledgements

This study was supported by the National Key R & D Program of China (Nos: 2018YFB0505500, 2018YFB0505502) and National Natural Science Foundation of China (Nos: 41771424, 41871299, 41631175). Dawei Han and Lu Zhuo were supported by Newton Fund via Natural Environment Research Council (NERC) and Economic and Social Research Council (ESRC) (NE/N012143/1).

References

Abt, S. , Wittier, R. , Taylor, A. and Love, D.: HUMAN STABILITY IN A HIGH FLOOD HAZARD ZONE1. JAWRA Journal of the American Water Resources Association, 25: 881-890, https://doi.org/10.1111/j.1752-1688.1989.tb05404.x, 1989.

Atta-Ur-Rahman, D.: Disaster risk management, 2014.

Bates, P. D., and De Roo, A. P. J.: A simple raster-based model for flood inundation simulation. Journal of hydrology, 236(1-2), 54-77, https://doi.org/10.1016/S0022-1694(00)00278-X, 2000.

Bates, P., Trigg, M., Neal, J., Dabrowa ,A.: LISFLOOD-FP User manual, Code release 5.9.6, School of Geographical Sciences, University of Bristol, University Road, Bristol, BS8 1SS, UK, 2013. Available online at University of https://www.bristol.ac.uk/media-library/sites/geography/migrated/documents/lisflood-manual-v5.9.6.pdf.

Bekhor, S., Ben-Akiva, M. E., and Ramming, M. S.: Evaluation of choice set generation algorithms for route choice models. Annals of Operations Research, 144(1), 235-247, https://doi.org/10.1007/s10479-006-0009-8, 2006.

Brunner, G. W.: HEC-RAS River Analysis System User's Manual Version 4.0. US Army Corps of Engineers, Hydrologic Engineering Center. Report CPD-68, 2008.

Cen, G., Shen, J., and Fan, R.: Research on rainfall pattern of urban design storm. Advances in Water Science, 9(1), 41-46, https://doi.org/10.14042/j.cnki.32.1309.1998.01.007, 1998.

Charley, W., Pabst, A., Peters, J.: The Hydrologic Modeling System (HEC-HMS): Design and Development Issues. Hydrological Engineering Center, US Army Corps of Engineers, Technical Paper No. 149, 1995.

Chen, Y., Zhou, H., Zhang, H., Du, G., and Zhou, J.: Urban flood risk warning under rapid urbanization. Environmental research, 139, 3-10, https://doi.org/10.1016/j.envres.2015.02.028, 2015.

Cools, M., Moons, E., Creemers, L., and Wets, G.: Changes in travel behavior in response to weather conditions: do type of weather and trip purpose matter?. Transportation Research Record: Journal of the Transportation Research Board, (2157), 22-28, https://doi.org/10.3141/2157-03, 2010.

566 Dai, Q., Han, D., Rico-Ramirez, M.A., and Srivastava, P.K.: Multivariate Distributed Ensemble
567 Generator: A new scheme for ensemble radar precipitation estimation over temperate
568 maritime climate, Journal of Hydrology, 511, 17-27, 2014.

569 Dai, Q., Rico-Ramirez, M.A., Han, D., Islam, T., and Liguori S.: Probabilistic radar rainfall
570 nowcasts using empirical and theoretical uncertainty models, Hydrological Processes, 29,
571 66-79, 2015.

572 Danish Hydraulic Institute (DHI).: MIKE SHE Water movement user manual. DHI Water &
573 Environment, 2000.

574 Dankers, R., and Feyen, L.: Climate change impact on flood hazard in Europe: An assessment
575 based on high‐resolution climate simulations. Journal of Geophysical Research:
576 Atmospheres, 113(D19), https://doi.org/10.1029/2007JD009719, 2008.

577 Dawson, R. J., Peppe, R., and Wang, M.: An agent-based model for risk-based flood incident
578 management. Natural hazards, 59(1), 167-189, https://doi.org/10.1007/s11069-011-9745-4,
579 2011.

580 DEFRA and Environment Agency.: Flood risks to people phase 1: R&D Technical Report
581 FD2317. DEFRA, London, 2003.

582 Dijkstra, E. W.: A note on two problems in connexion with graphs. Numerische mathematik,
583 1(1), 269-271, 1959.

584 Drobot, S. D., Benight, C., and Gruntfest, E. C.: Risk factors for driving into flooded roads.
585 Environmental Hazards, 7(3), 227-234, https://doi.org/10.1016/j.envhaz.2007.07.003, 2007.

586 Gain, A. K., Mojtahed, V., Biscaro, C., Balbi, S., and Giupponi, C.: An integrated approach of
587 flood risk assessment in the eastern part of Dhaka City. Natural Hazards, 79(3), 1499-1530,
588 https://doi.org/10.1007/s11069-015-1911-7, 2015.

589 Geopandas: http://geopandas.org/, 2018.

590 Guo, E., Zhang, J., Ren, X., Zhang, Q., and Sun, Z.: Integrated risk assessment of flood disaster
591 based on improved set pair analysis and the variable fuzzy set theory in central Liaoning
592 Province, China. Natural hazards, 74(2), 947-965, https://doi.org/10.1007/s11069-014-
593 1238-9, 2014.

594 Hammond, M. J., Chen, A. S., Djordjević, S., Butler, D., and Mark, O.: Urban flood impact
595 assessment: A state-of-the-art review. Urban Water Journal, 12(1), 14-29,
596 https://doi.org/10.1080/1573062X.2013.857421, 2015.

597 Havnø, K., Madsen, M. N., and Dørge, J.: MIKE 11–a generalized river modelling package.
598 Computer models of watershed hydrology, 733-782, 1995.

599 Horritt, M. S., and Bates, P. D.: Evaluation of 1D and 2D numerical models for predicting river
600 flood inundation. Journal of hydrology, 268(1-4), 87-99, https://doi.org/10.1016/S0022-
601 1694(02)00121-X, 2002.

602 Huang, H., Fan, Y., Yang, S., Li, W., Guo, X., Lai W., and Wang H.: A multi-agent based
603 theoretical model for dynamic flood disaster risk assessment. Geographical Research,
604 34(10):1875-1886, https://doi.org/10, 1875-1886, 10.11821/dlyj20151006, 2015.

IPCC.: Summary for Policymakers. In: Managing the Risks of Extreme Events and Disasters to Advance Climate Change Adaptation. A Special Report of Working Groups I and II of the Intergovernmental Panel on Climate Change. Cambridge University Press, Cambridge, UK, and New York, NY, USA, pp. 3-21, 2012.

Johnstone, M. A.: Life safety modelling framework and performance measures to assess community protection systems: application to tsunami emergency preparedness and dam safety management, Ph.D. thesis, University of British Columbia, 2012.

Jonkman, S. N., and Kelman, I.: An analysis of the causes and circumstances of flood disaster deaths. Disasters, 29(1), 75-97, https://doi.org/10.1111/j.0361-3666.2005.00275.x, 2005.

Jonkman, S. N., and Penning‐Rowsell, E.: Human Instability in Flood Flows 1. JAWRA Journal of the American Water Resources Association, 44(5), 1208-1218, https://doi.org/10.1111/j.1752-1688.2008.00217.x, 2008.

Karvonen, R. A., Hepojoki, A., Huhta, H. K., and Louhio, A.: The use of physical models in dam-break analysis. RESCDAM Final Report. Helsinki University of Technology, Helsinki, Finland, 2000.

Liang, Y., Wen, J., Du, S., Xu, H., and Yan J.: Spatial-temporal Distribution Modeling of Population and its Applications in Disaster and Risk Management. Journal of Catastrophology, 30(04):220-228, https://doi.org/ 10.3969/j.issn.1000-811X.2015.04.038, 2015.

Lind, N., Hartford, D., and Assaf, H.: Hydrodynamic models of human stability in a flood 1. JAWRA Journal of the American Water Resources Association, 40(1), 89-96, https://doi.org/10.1111/j.1752-1688.2004.tb01012.x, 2004.

Lindberg, S., Nielsen, J. B., and Carr, R.: An integrated PC-modelling system for hydraulic analysis of drainage systems. In Watercomp'89: The First Australasian Conference on Technical Computing in the Water Industry; Preprints of Papers (p. 127). Institution of Engineers, Australia, 1989.

Lü, G., Batty, M., Strobl, J., Lin, H., Zhu, A. X., and Chen, M.: Reflections and speculations on the progress in Geographic Information Systems (GIS): a geographic perspective. International Journal of Geographical Information Science, 1-22, https://doi.org/10.1080/13658816.2018.1533136, 2018.

Mahe, G., Paturel, J. E., Servat, E., Conway, D., and Dezetter, A.: The impact of land use change on soil water holding capacity and river flow modelling in the Nakambe River, Burkina-Faso. Journal of Hydrology, 300(1-4), 33-43, https://doi.org/10.1016/j.jhydrol.2004.04.028, 2005.

Mansur, A. V., Brondízio, E. S., Roy, S., Hetrick, S., Vogt, N. D., and Newton, A.: An assessment of urban vulnerability in the Amazon Delta and Estuary: a multi-criterion index of flood exposure, socio-economic conditions and infrastructure. Sustainability Science, 11(4), 625-643, https://doi.org/10.1007/s11625-016-0355-7, 2016.

Matplotlib: https://matplotlib.org/, 2018.

644 Moel, H. D., Aerts, J. C., and Koomen, E.: Development of flood exposure in the Netherlands
645 during the 20th and 21st century. Global Environmental Change, 21(2), 620-627,
646 https://doi.org/10.1016/j.gloenvcha.2010.12.005, 2011.

647 Nasiri, H., Mohd Yusof, M.J., and Mohammad Ali, T.A.: An overview to flood vulnerability
648 assessment methods. Sustain. Water Resour. Manag., 2: 331,
649 https://doi.org/10.1007/s40899-016-0051-x, 2016.Papinski, D., Scott, D. M., and Doherty,
650 S. T.: Exploring the route choice decision-making process: A comparison of planned and
651 observed routes obtained using person-based GPS. Transportation research part F: traffic
652 psychology and behaviour, 12(4), 347-358, https://doi.org/10.1016/j.trf.2009.04.001, 2009.

653 Parker, D., Fordham, M., Tunstall, S., and Ketteridge, A. M.: Flood warning systems under stress
654 in the United Kingdom. Disaster Prevention and Management: An International Journal,
655 4(3), 32-42, https://doi.org/10.1108/09653569510088050, 1995.

656 Python: https://www.python.org/, 2018.

657 Qt: https://www.qt.io/, 2018.

658 Ramming, M. S.: Network knowledge and route choice, Unpublished Ph. D. Thesis,
659 Massachusetts Institute of Technology, 2001.

660 Rossman, L. A.: Storm water management model user's manual Version 5.1 EPA-600/R-
661 14/413b[z]. National Risk Management Laboratory Laboratory Office of Research and
662 Development U. S. Environmental Protection Agency, 2015. Available online at
663 https://nepis.epa.gov/Exe/ZyPDF.cgi/P100N3J6.PDF?Dockey=P100N3J6.PDF

664 Röthlisberger, V., Zischg, A. P., and Keiler, M.: Identifying spatial clusters of flood exposure to
665 support decision making in risk management. Science of the total environment, 598, 593-
666 603, https://doi.org/10.1016/j.scitotenv.2017.03.216, 2017.

667 Ruin, I., Gaillard, J. C., and Lutoff, C.: How to get there? Assessing motorists' flash flood risk
668 perception on daily itineraries. Environmental hazards, 7(3), 235-244,
669 https://doi.org/10.1016/j.envhaz.2007.07.005, 2007.

670 Shabou, S., Ruin, I., Lutoff, C., Debionne, S., Anquetin, S., Creutin, J. D., and Beaufils, X.:
671 MobRISK: a model for assessing the exposure of road users to flash flood events. Natural
672 Hazards and Earth System Sciences, 17(9), 1631, https://doi.org/10.5194/nhess-17-1631-
673 2017, 2017.

674 Shi, P.: Theory and practice of disaster study. Journal of Natural Disasters, 4, 8-19, 1996.

675 Terti, G., Ruin, I., Anquetin, S., and Gourley, J. J.: Dynamic vulnerability factors for impact-
676 based flash flood prediction. Natural Hazards, 79(3), 1481-1497.
677 https://doi.org/10.1007/s11069-015-1910-8, 2015.

678 Visual studio code: https://code.visualstudio.com/, 2018.

679 Wan, H., Wang, J.: Analysis of Public Adaptive Behaviors to Drought and Flood Disasters in
680 Middle Reaches of Weihe River:A Case Study on Qishan County of Shaanxi Province. Acta
681 Agriculturae Jiangxi, https://doi.org/10.19386/j.cnki.jxnyxb.2017.05.21, 2017.

682 Weis, S. W. M., Agostini, V. N., Roth, L. M., Gilmer, B., Schill, S. R., Knowles, J. E., and
683 Blyther, R.: Assessing vulnerability: an integrated approach for mapping adaptive capacity,

sensitivity, and exposure. Climatic Change, 136(3-4), 615-629, https://doi.org/10.1007/s10584-016-1642-0, 2016.

Werren, G., Reynard, E., Lane, S. N., and Balin, D.: Flood hazard assessment and mapping in semi-arid piedmont areas: a case study in Beni Mellal, Morocco. Natural Hazards, 81(1), 481-511, https://doi.org/10.1007/s11069-015-2092-0, 2016.

Yang, X., Yue, W., and Gao, D.: Spatial improvement of human population distribution based on multi-sensor remote-sensing data: an input for exposure assessment. International journal of remote sensing, 34(15), 5569-5583, https://doi.org/10.1080/01431161.2013.792970, 2013.

Yin, Z.: Research of urban natural disaster risk assessment and case study, Ph.D. thesis, East china normal university, Shanghai, China, 2009.

Yin, J., Yu, D., and Wilby, R.: Modelling the impact of land subsidence on urban pluvial flooding: A case study of downtown Shanghai, China. Science of the Total Environment, 544, 744-753, https://doi.org/10.1016/j.scitotenv.2015.11.159, 2016a.

Yin, W., Yu, H., Cui, S., and Wang, J.: Review on methods for estimating the loss of life induced by heavy rain and floods. Progress in Geography, 35(2), 148-158, https://doi.org/10.18306/dlkxjz.2016.02.002, 2016b.

Figure 1. Location of the study area (left) and a digital elevation model indicating the specific details of the study area (right).

Figure 2. Overview of the dynamic exposure simulation to urban flooding.

Figure 3. Rainfall simulation results based on the CHM method, and observational data used for fluvial flood simulation.

Figure 4. A synthetic daily routine generated from the travel survey and census data for an employed male agent aged 18–60 years.

Figure 5. Activity patterns for an employed male agent aged 18–60 years and highly educated during disaster scenarios. (a) Bad weather (weekday) (b) Warning (weekday) (c) Bad weather (weekend) (d) Warning (weekend).

Figure 6. Block numbers of different block types.

Figure 7. Spatial distribution of blocks.

Figure 8. Agent types for daily and disaster scenarios. Daily scenarios refer to S1, S2, S7, and S8. Others are disaster scenarios.

Figure 9. Map of accumulated water depths and velocities. T means time here.

Figure 10. Changes in the surface water depths and velocities for eight severely flooded areas. The “dep” indicates water depth, and “vel” indicates water velocity.

Figure 11. Map of the flooded area indicating the flooding simulation and the real flood in 2014. The information for the flooded area was provided by Lishui City Housing and Urban-Rural Construction Bureau.

Figure 12. Population changes in blocks and roads for the six scenarios.

Figure 13. Population distribution for the six scenarios. T means time here.

Figure 14. Changes in the population exposure of two blocks for the 12 scenarios. Block 168 was a recreational area, and Block 6 was a residential area.

Figure 15. Changes in road and building exposures in severely flooded blocks. The exposed road length and building area represent road and building exposures, respectively.

Figure 16. Map of road and building exposures. T means time here.

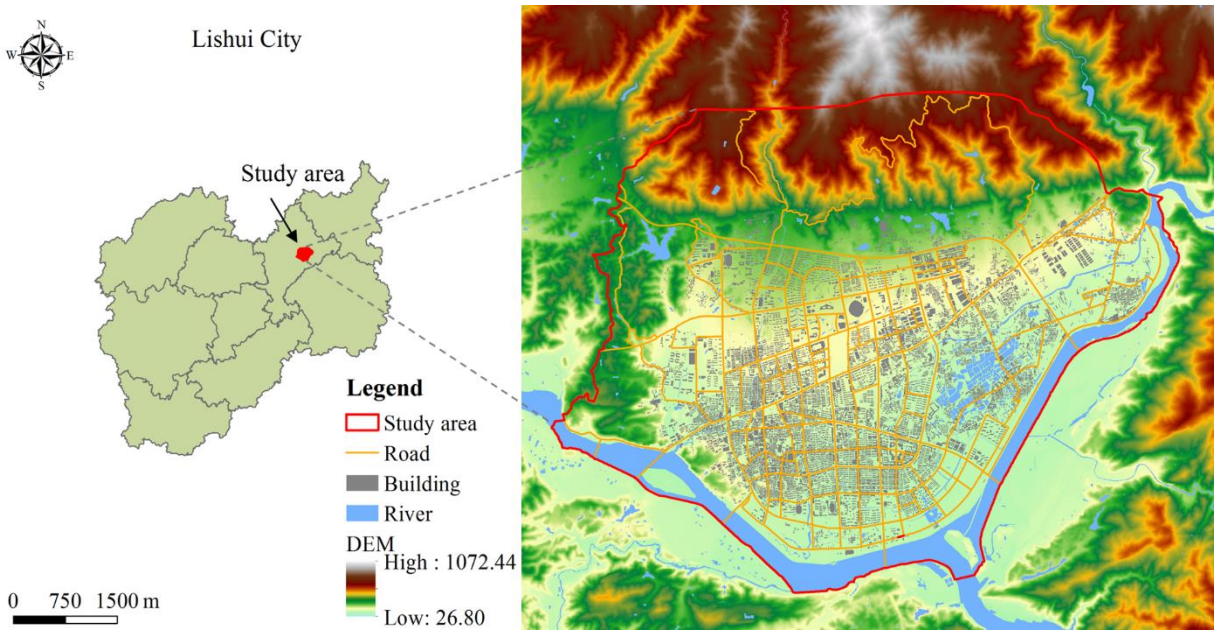

Figure 1. Location of the study area (left) and a digital elevation model indicating the specific details of the study area (right).

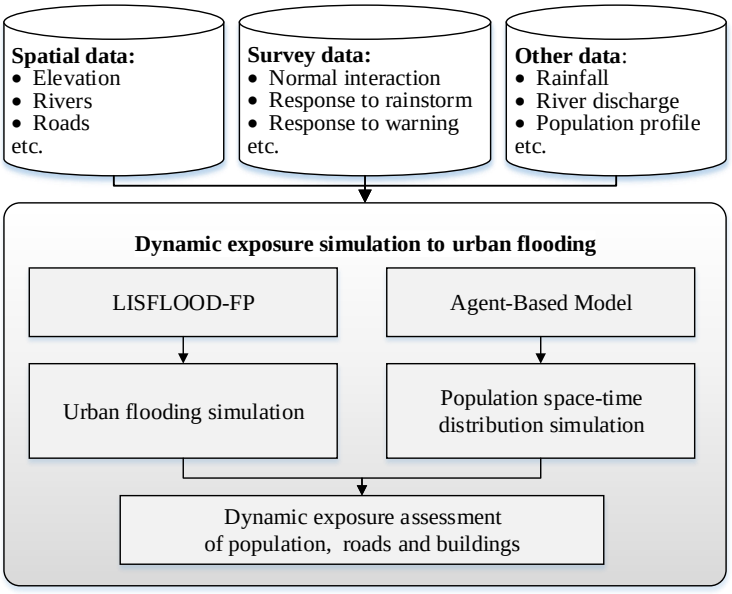

731

732 **Figure 2.** Overview of the dynamic exposure simulation to urban flooding.

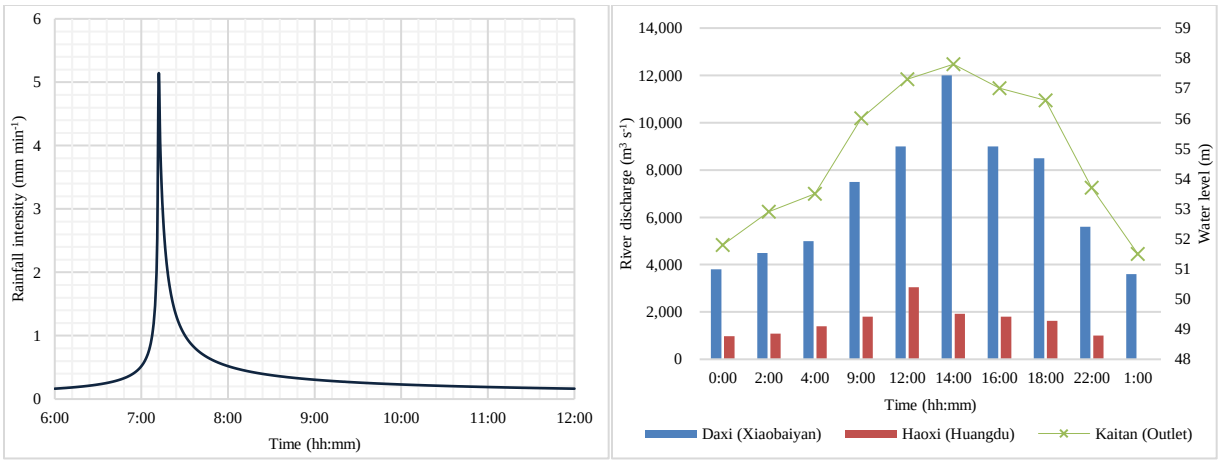

(a) Rainfall simulation data (b) Observational data

Figure 3. Rainfall simulation results based on the CHM method, and observational data used for fluvial flood simulation.

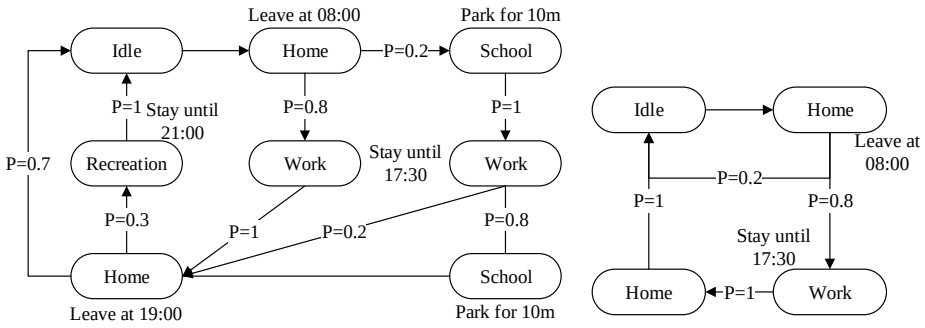

(a) Activity on weekdays (b) Activity on weekends

Figure 4. A synthetic daily routine generated from the travel survey and census data for an employed male agent aged 18–60 years.

741

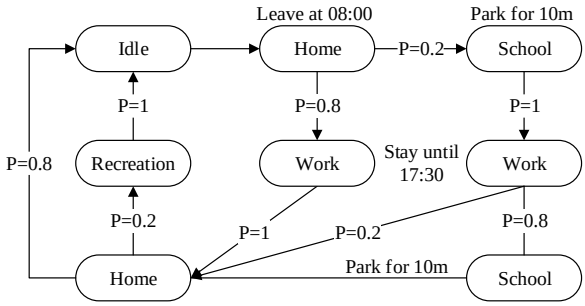

742 (a) Bad weather (weekday)

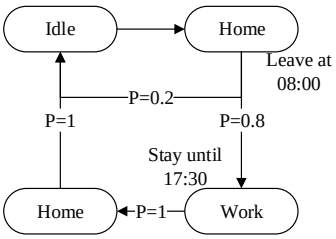

(b) Warning (weekday)

743

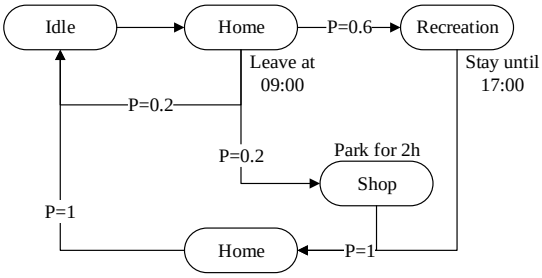

744 (c) Bad weather (weekend)

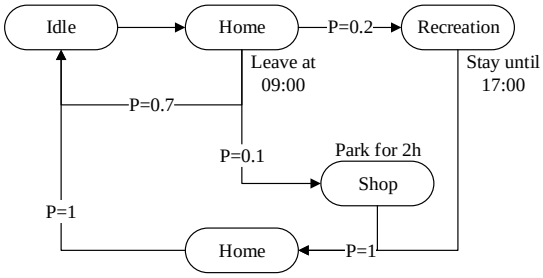

(d) Warning (weekend)

745 **Figure 5.** Activity patterns for an employed male agent aged 18–60 years and highly educated
746 during disaster scenarios. (a) Bad weather (weekday) (b) Warning (weekday) (c) Bad weather
747 (weekend) (d) Warning (weekend).

748

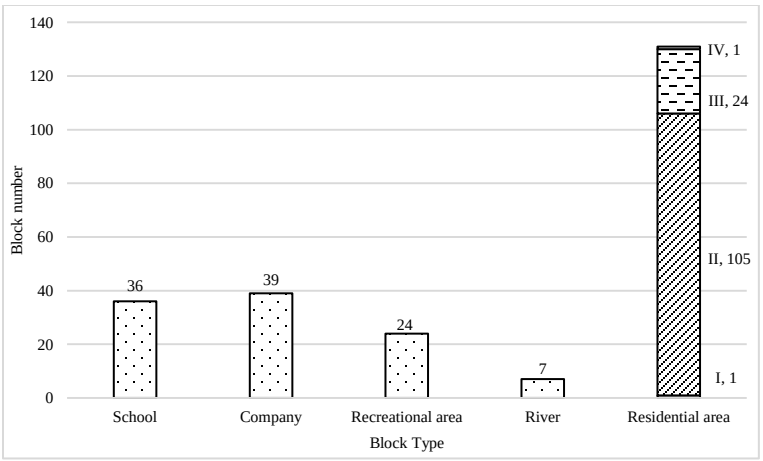

749

750 **Figure 6.** Block numbers of different block types.

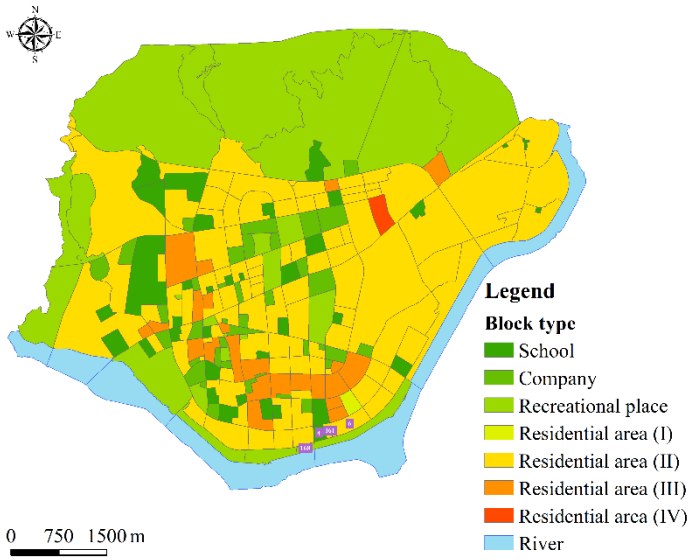

751

752 **Figure 7.** Spatial distribution of blocks.

753

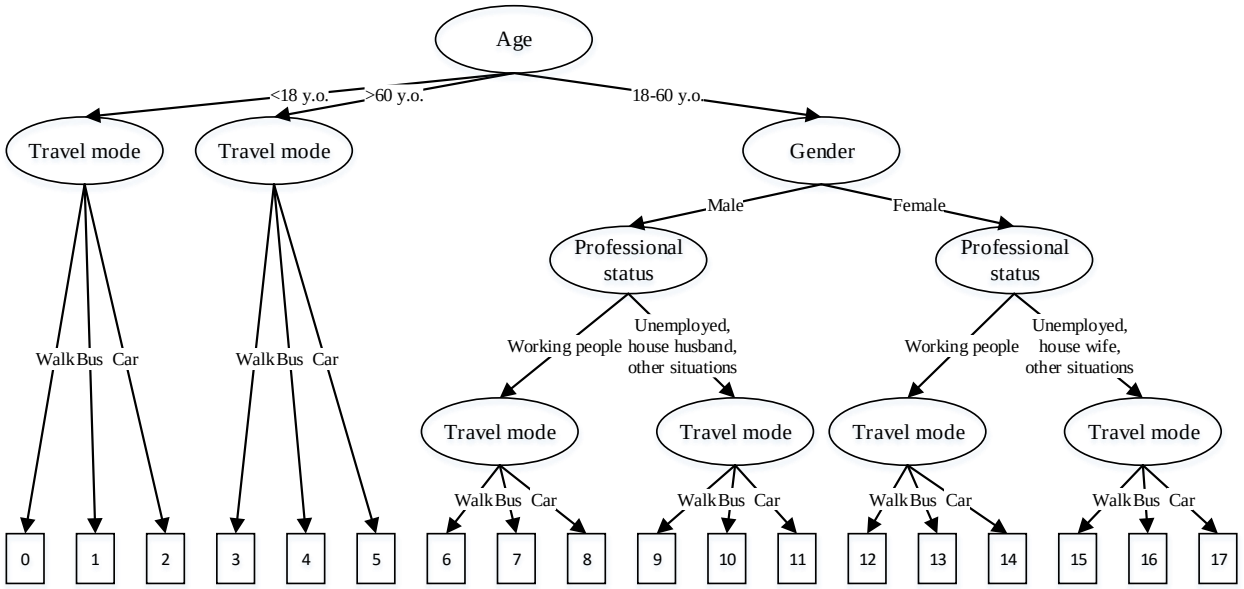

(a) Agent types for daily scenarios

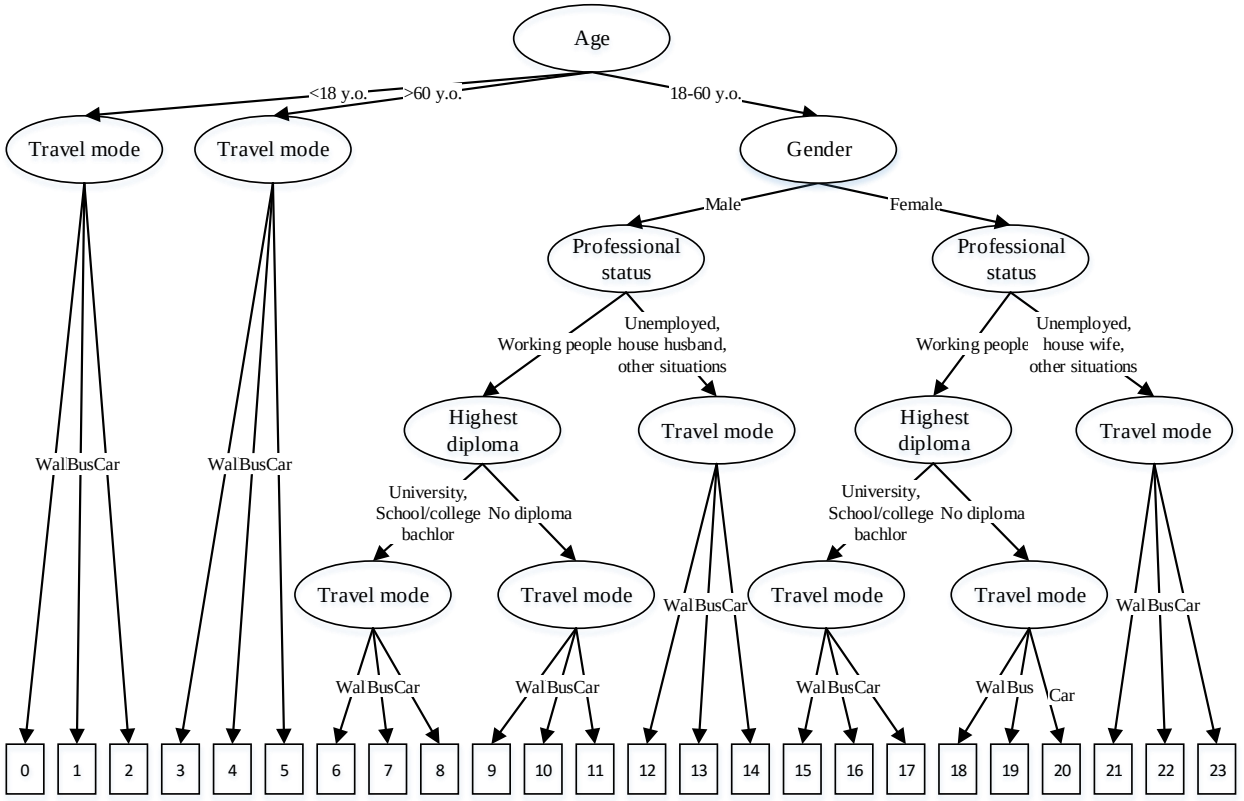

(b) Agent types for disaster scenarios

Figure 8. Agent types for daily and disaster scenarios. Daily scenarios refer to S1, S2, S7, and S8. Others are disaster scenarios.

760

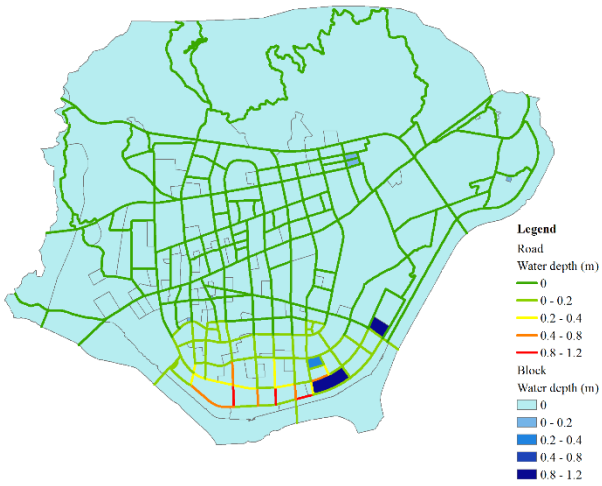

761 (a) Water depth (pluvial flood, T = 15:00)

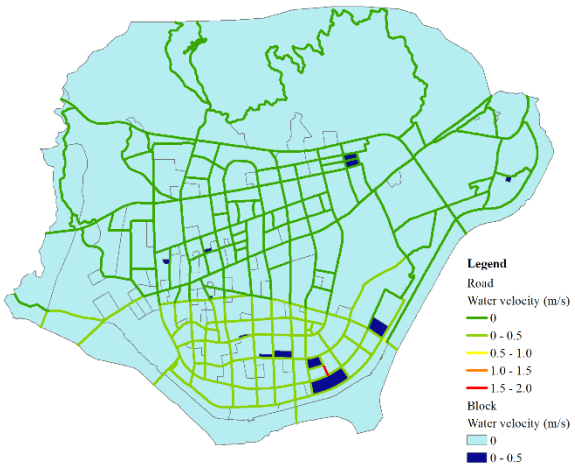

(b) Water velocity (pluvial flood, T = 08:00)

762

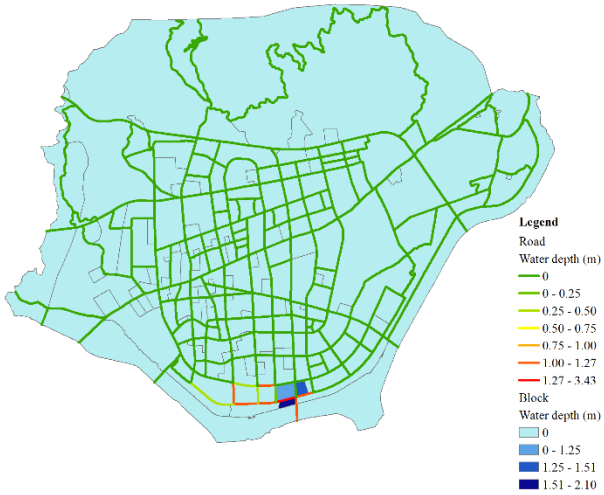

763 (c) Water depth (fluvial flood, T = 16:00)

(d) Water velocity (fluvial flood, T = 16:00)

764 **Figure 9.** Map of accumulated water depths and velocities. T means time here.

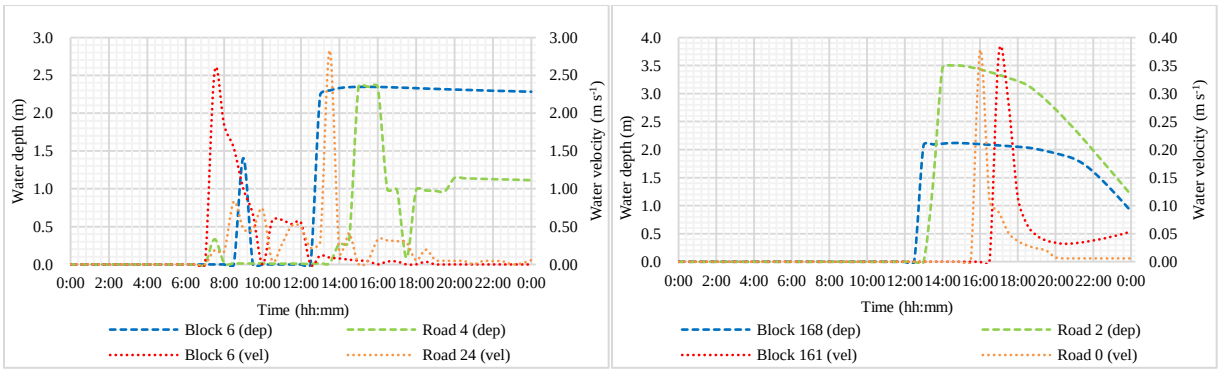

765

766 (a) Pluvial flood (b) Fluvial flood

767 **Figure 10.** Changes in the surface water depths and velocities for eight severely flooded areas.

768 The “dep” indicates water depth, and “vel” indicates water velocity.

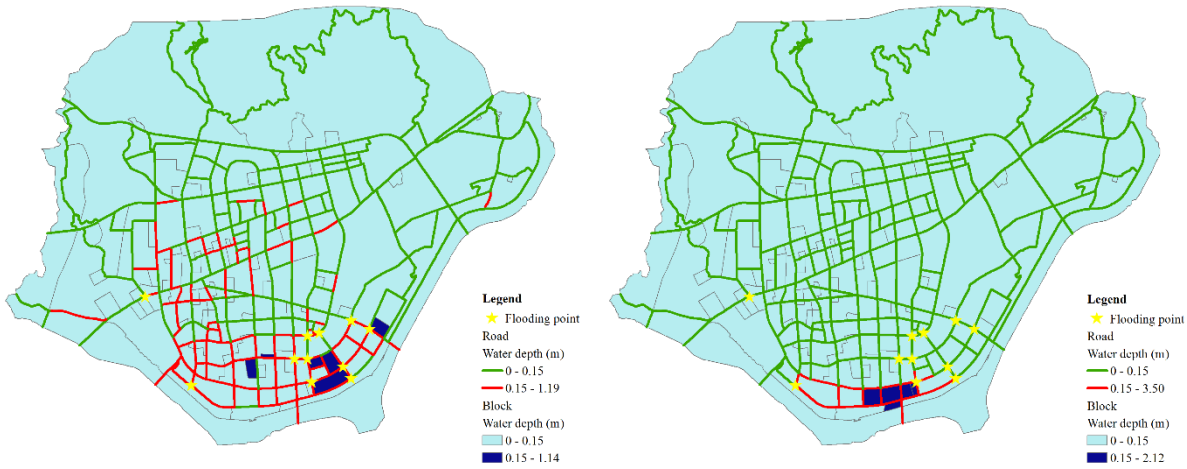

(a) Pluvial flood (b) Fluvial flood

Figure 11. Map of the flooded area indicating the flooding simulation and the real flood in 2014. The information for the flooded area was provided by Lishui City Housing and Urban-Rural Construction Bureau.

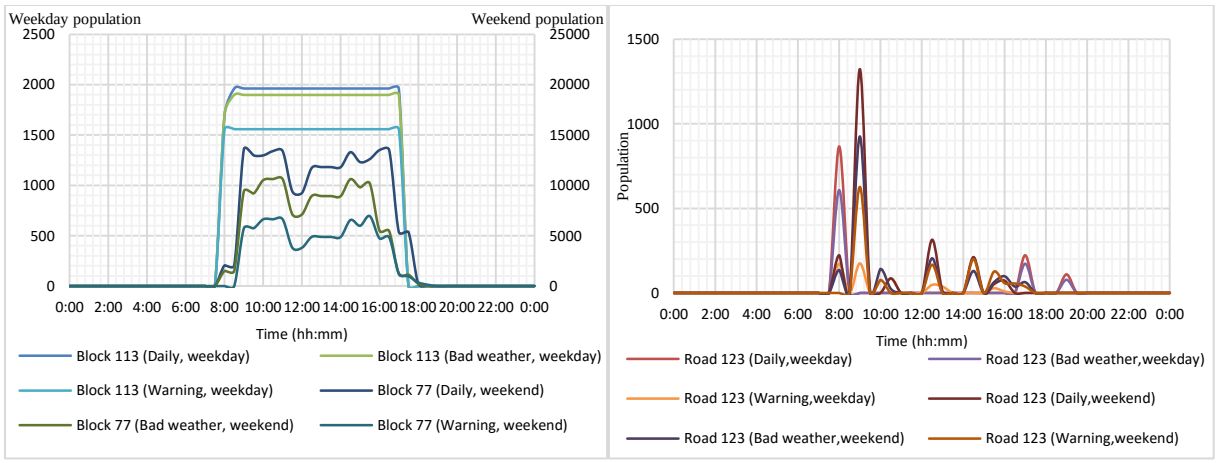

(a) Block (b) Road

Figure 12. Population changes in blocks and roads for the six scenarios.

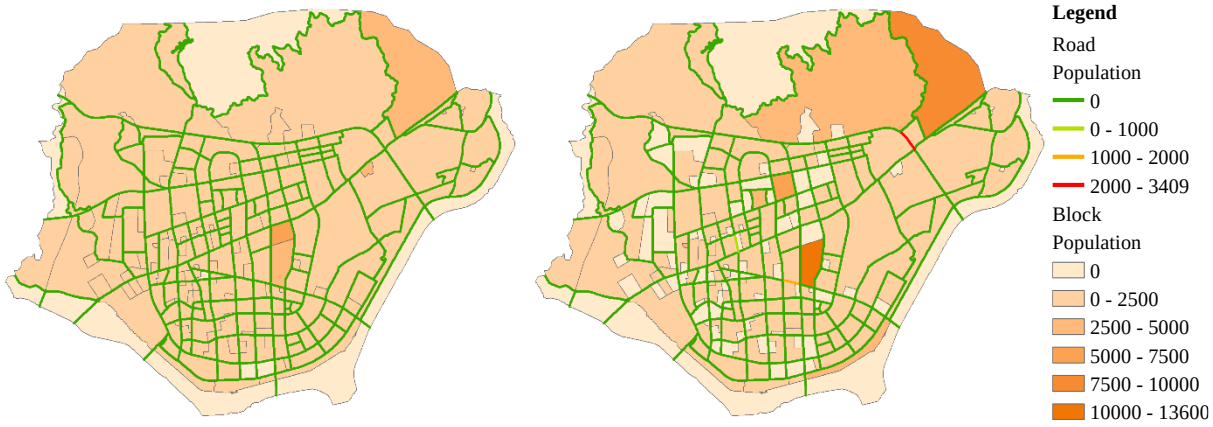

(a) Daily, weekday (T = 09:00) (b) Daily, weekend (T = 09:00)

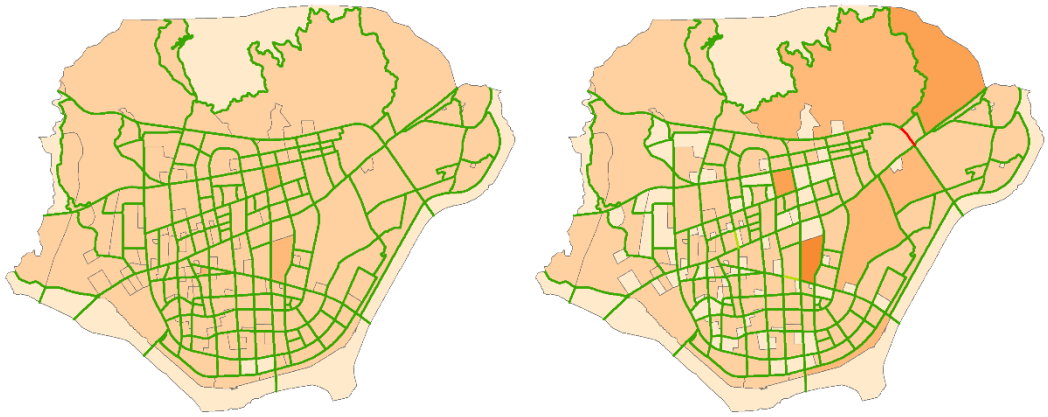

(c) Bad weather, weekday (T = 09:00) (d) Bad weather, weekend (T = 09:00)

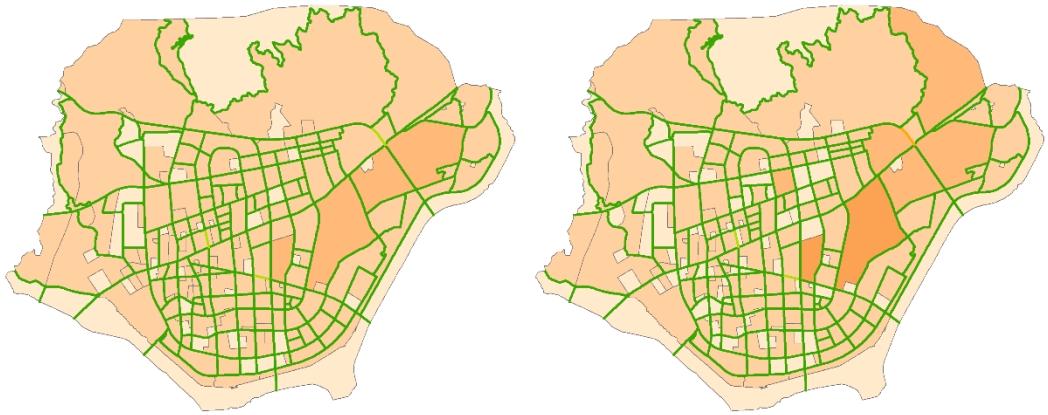

(e) Warning, weekday (T = 09:00) (f) Warning, weekend (T = 09:00)

Figure 13. Population distribution for the six scenarios. T means time here.

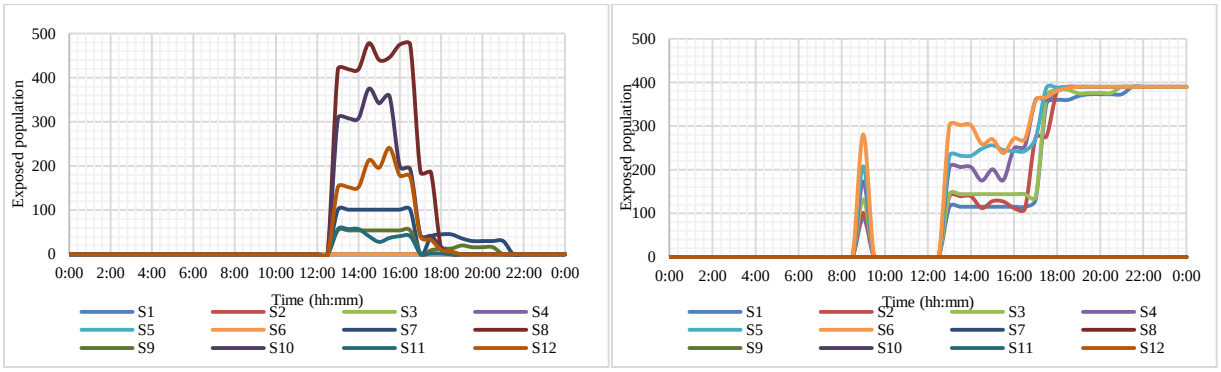

(a) Population exposure (Block 168) (b) Population exposure (Block 6)

Figure 14. Changes in the population exposure of two blocks for the 12 scenarios. Block 168 was a recreational area, and Block 6 was a residential area.

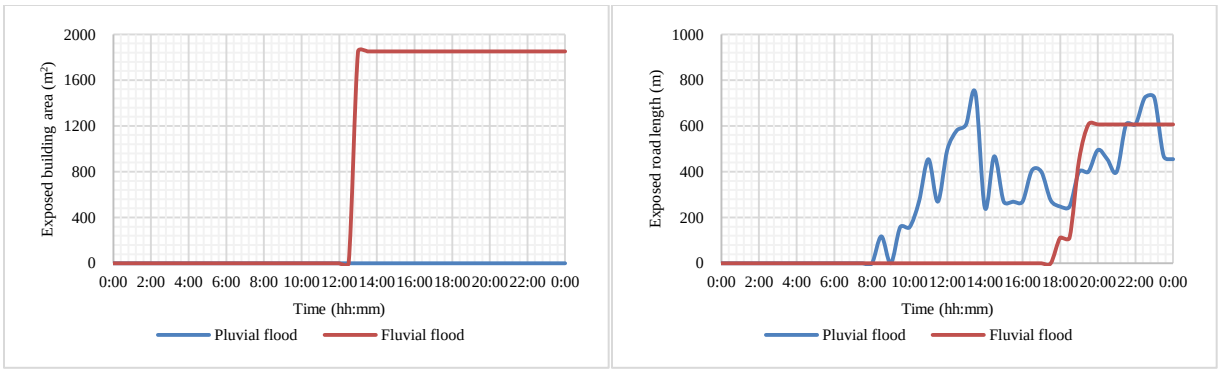

789

790 (a) Exposed building area (Block 168) (d) Exposed road length (Block 6)

791 **Figure 15.** Changes in road and building exposures in severely flooded blocks. The exposed road
792 length and building area represent road and building exposures, respectively.

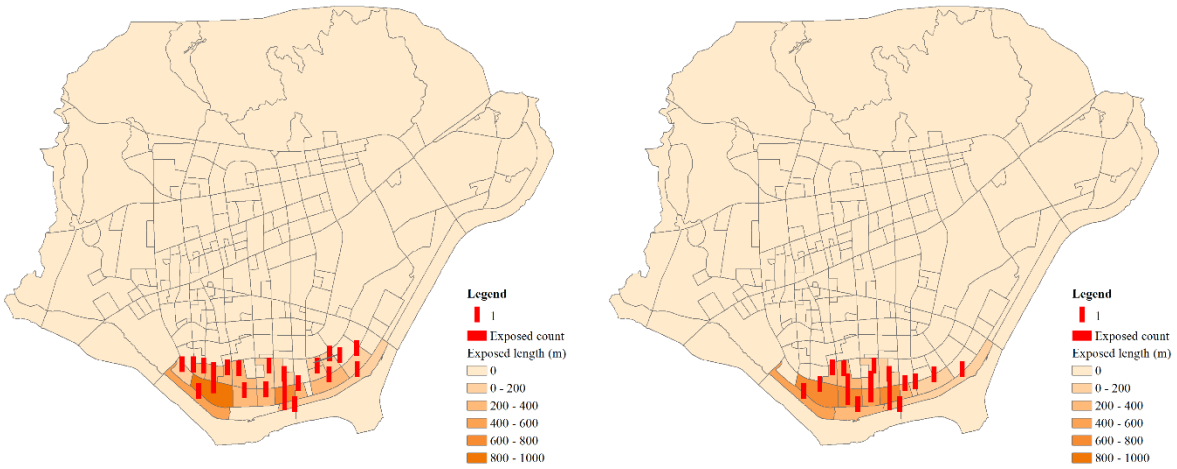

793

794 (a) Road exposure (pluvial flood, T = 18:30) (b) Road exposure (fluvial flood, T = 18:30)

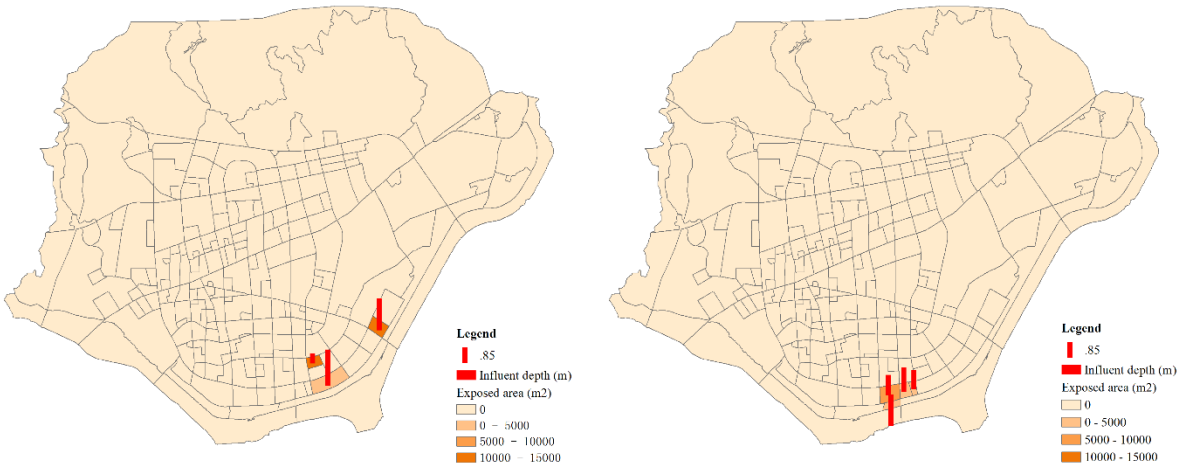

795

796 (c) Building exposure (pluvial flood, T = 18:30) (d) Building exposure (fluvial flood, T = 18:30)

797 **Figure 16.** Map of road and building exposures. T means time here.

803 **Table 1.** Data used in this study.

Data	Source	Time	Use
Digital elevation model	Local government	2013	Topography (regular square grids with a 5 m resolution)
Basic geographic data	Local government	2015	Locations of rivers, roads, and buildings
Hydrological data	Local government	Aug 20, 2014	River discharge and water level
1 km grid population data	National Earth System Science Data Sharing Infrastructure, National Science & Technology Infrastructure of China (http://www.geodata.cn)	2010	Number of residents per grid in the study area
Population profile	Lishui Statistical Yearbook and Liandu Yearbook (http://tjj.lishui.gov.cn)	2014	Gender, age, education level, employment, and travel mode profiles were used to classify agent groups
Travel survey data	Face-to-face questionnaire surveys	July 8, 2018 to July 14, 2018	Social characteristics and daily activities of 500 residents
Traffic flow data	Local government	June 24, 2017 to July 7, 2017	Number of vehicles passing through a node within one hour at four intersections from June 24, 2017 to July 7, 2017 in this area
Water accumulation points	Local government (http://www.zjjs.com.cn)	Aug 20, 2014	Location

804

805 **Table 2**. Parameter values for the rainstorm intensity formula.

Parameter	Value
A	1265.3
b	5.919
c	0.587
n	0.611

806

807 **Table 3**. Parameter variations used in the simulation scenarios.

Scenarios	Flooding type	Human behavior	Weekdays or weekends
S1	Pluvial flood	Daily	Weekdays
S2	Pluvial flood	Daily	Weekends
S3	Pluvial flood	Bad weather	Weekdays
S4	Pluvial flood	Bad weather	Weekends
S5	Pluvial flood	Warning	Weekdays
S6	Pluvial flood	Warning	Weekends
S7	Fluvial flood	Daily	Weekdays
S8	Fluvial flood	Daily	Weekends
S9	Fluvial flood	Bad weather	Weekdays
S10	Fluvial flood	Bad weather	Weekends
S11	Fluvial flood	Warning	Weekdays
S12	Fluvial flood	Warning	Weekends

808

809 **Table 4**. Sociodemographic characteristics of the study area population.

Variables	Groups	Percentage (%)
Gender	Male	50.43
	Female	49.57
Age	0-17	18.73
	18-60	63.34
	>60	17.93
Professional status	Employed	55.77
	Unemployed	44.23
Education level	University, school-college, bachelor	14.46
(Highest diploma)	No diploma	85.54
Travel mode	Walk	25.24
	Bus	43.06
	Car	31.70

810 Note: Data are drawn from the 2015 Lishui Statistical Yearbook and 2015 Liandu Yearbook.

Table 5. Building step heights for different block types.

No	Block type	Building type	Building step height
1	Residential area I	Garden house, villa	0.35 m (with > 9 floors, 0.60 m)
2	Residential area II	High-rise apartments and new village houses (before 1988); new residential quarters and commercial houses (after 1988)	0.35 m (with > 9 floors, 0.60 m)
3	Residential area III	New and old lane homes, three types of staff housing	0.10 m
4	Residential area IV	Shed house	0.05 m
5	School	Educational building	0.35 m (with > 9 floors, 0.60 m)
6	Company	Office building	0.35 m (with > 9 floors, 0.60 m)
7	Recreational area	Public buildings for business, culture, sports, and other uses	0.35 m (with > 9 floors, 0.60 m)

811

Table 6. Traffic flow and population simulation results during peak hours on weekdays.

Road junction	Time	Sim.	Obs.	Deviation ratio
LQ-KF	8:00–9:00	319	366	-12.84%
LQ-KF	17:00–18:00	602	591	1.86%
LQ-HY	8:00–9:00	353	398	-11.31%
LQ-HY	17:00–18:00	740	731	1.23%
LQ-ZJ	8:00–9:00	381	369	3.25%
LQ-ZJ	17:00–18:00	824	814	1.23%
LT-ZJ	8:00–9:00	531	508	4.53%
LT-ZJ	17:00–18:00	994	938	5.97%

812

Table 7. Traffic flow and population simulation results during peak hours on weekends.

Road junction	Time	Sim.	Obs.	Deviation ratio
LQ-KF	8:00–9:00	523	529	-1.13%
LQ-KF	17:00–18:00	659	693	-4.91%
LQ-HY	8:00–9:00	761	725	4.97%
LQ-HY	17:00–18:00	822	790	4.05%
LQ-ZJ	8:00–9:00	651	638	2.04%
LQ-ZJ	17:00–18:00	825	873	-5.50%
LT-ZJ	8:00–9:00	778	712	9.27%
LT-ZJ	17:00–18:00	1083	1132	-4.33%

813